

The interplay between a galactic bar and a supermassive black hole: nuclear fueling in a sub-parsec resolution galaxy simulation

Eric Emsellem,^{1,2*} Florent Renaud³, Frédéric Bournaud³, Bruce Elmegreen⁴, Françoise Combes⁵, Jared M. Gabor³

¹European Southern Observatory, Karl-Schwarzschild-Str. 2, 85748 Garching, Germany

²Université Lyon 1, Observatoire de Lyon, Centre de Recherche Astrophysique de Lyon
and Ecole Normale Supérieure de Lyon, 9 avenue Charles André, F-69230 Saint-Genis Laval, France

³Laboratoire AIM Paris-Saclay, CEA/IRFU/SAp – CNRS – Université Paris Diderot, 91191 Gif-sur-Yvette Cedex, France

⁴IBM Research Division, T.J. Watson Research Center, 1101 Kitchawan Road, Yorktown Heights, NY 10598, USA

⁵Observatoire de Paris, LERMA, CNRS: UMR8112, 61 Av. de l'Observatoire, 75014 Paris, France

27 October 2014

ABSTRACT

We study the connection between the large-scale dynamics and the gas fueling toward a central black hole via the analysis of a Milky Way-like simulation at sub-parsec resolution. This allows us to follow a set of processes at various scales (e.g., the triggering of inward gas motion towards inner resonances via the large-scale bar, the connection to the central black hole via mini spirals) in a self-consistent manner. This simulation provides further insights on the role of shear for the inhibition of star formation within the bar in regions with significant amount of gas. We also witness the decoupling of the central gas and nuclear cluster from the large-scale disc, via interactions with the black hole. This break of symmetry in the mass distribution triggers the formation of gas clumps organised in a time-varying 250 pc ring-like structure, the black hole being offset by about 70 pc from its centre. Some clumps form stars, while most get disrupted or merge. Supernovae feedback further creates bubbles and filaments, some of the gas being expelled to 100 pc or higher above the galaxy plane. This helps remove angular momentum from the gas, which gets closer to the central dark mass. Part of the gas raining down is being accreted, forming a 10 pc polar disc-like structure around the black hole, leading to an episode of star formation. This gives rise to multiple stellar populations with significantly different angular momentum vectors, and may lead to a natural intermittence in the fueling of the black hole.

Key words: galaxies: evolution – galaxies: kinematics and dynamics – hydrodynamics – Galaxy: kinematics and dynamics – Galaxy: nucleus – methods: numerical

1 INTRODUCTION

One of the most common but daunting challenges for simulating astrophysical objects is to be able to properly treat various physical processes and their associated scales simultaneously. The onset and impact of gas fueling within a few hundreds of parsecs driven by a kpc-scale bar in a galaxy (Roberts et al. 1979; Shlosman et al. 1989; Athanassoula 1992; Jogee et al. 2005; Haan et al. 2009; Cisternas et al. 2013; Combes et al. 2014; Garcia-Burillo et al. 2014) is an excellent illustration of a problem which requires pushing our models and facilities to their limits. Assuming that we ignore the interactions with the galactic environment and the associated infall and outflows of material, angular momentum, and energy, probing the formation and evolution of the bar requires to follow the large-scale dynamics, hence the disc scale with tens of kiloparsecs, and

its potential coupling with star formation and feedback, therefore down to sub-parsec regions if we are to resolve the associated local quasi-isotropic turbulent motions (Bournaud et al. 2010).

In a gas-rich galaxy, we expect a rapidly time-varying system with strong coupling from processes such as global and local instabilities, turbulence (3D and inverse 2D) cascades and star formation (Elmegreen 1993; Padoan & Nordlund 2002; Levine et al. 2008; Bournaud et al. 2010; Padoan & Nordlund 2011; Hopkins & Quataert 2010a). We also expect the interplay between the underlying frequencies set up by the tumbling and evolving potential (pattern speed of the bar and spirals) and the local frequencies (e.g., epicycle) to have a strong impact on how and where the gas exchanges angular momentum or forms stars (see e.g. Combes 2001; Jogee 2006). Resonances will thus shape the orbital structure of the galaxy and are therefore critical ingredients to understand the overall evolution (Binney et al. 1991; Athanassoula 1992; Wada & Habe 1995; Englmaier & Shlosman 2000; Stark et al. 2004).

* E-mail: eric.emsellem@eso.org

In that context, the presence (or absence) of a supermassive black hole at the centre of the galaxy will play a prominent role, as it significantly modifies both the profile and shape of the potential in its close environment (Englmaier & Shlosman 2000; Maciejewski 2004a), and consequently the presence and location of the inner resonances (e.g., the Inner Lindblad Resonance), and also act as a massive particle among a sea of stars and gas clouds (Merritt 2010). The feedback from the active nucleus, when included, could also affect the evolution of the system both locally and globally (Haas et al. 2013; Gabor & Bournaud 2014; Choi et al. 2014). Molecular gas structures such as spirals and outflows in the nuclear regions of three local barred galaxies have been mapped recently at high angular resolution; they suggest the presence of high torques that can drive accretion to a central black hole (Combes et al. 2013, 2014; Garcia-Burillo et al. 2014).

In the present paper, we are making use of a Milky-Way like simulation to probe the coupling between the gas fueling driven by a large-scale bar and the central region surrounding a supermassive black hole. For such a study, we focus on an isolated galactic system to further understand the physical ingredients which may indeed associate the large-scale evolution in the disc with the very central structures. We also focus on the dynamical processes, as well as on the associated star formation and its feedback, thus ignoring the more global cosmological context or the active galactic nucleus’ (AGN) feedback.

In the next Section, we briefly describe the ingredients for such a simulation. In Section 3, we present the first results, following on the formation and evolution of the bar and the triggered gas fueling leading to the emergence of complex central structures in the close environment of the black hole. In Section 4, we briefly discuss these results, adding some perspectives for follow-up studies. A summary of the structures we observe in the simulation is provided in Fig. 13.

2 THE MILKY-WAY SIMULATION

We use the Milky Way-like galaxy simulation presented in (Renaud et al. 2013, thereafter R+13), and of which the main aspects are summarized below. A disc galaxy is modeled in three dimensions, with live dark matter halo and stellar components rendered with 60 millions particles. In addition, a super massive black hole of $4 \times 10^6 M_\odot$ is initially set at the center of the galaxy: the black hole is treated as a single massive particle with no direct accretion, growth or associated feedback. For these components (dark matter, primordial stars and super-massive black hole), the gravitational potential is computed using a particle-mesh technique with the resolution (i.e. softening) of 3 pc, as to limit the noise due to individual particles. The gaseous component is setup on a grid, which follows the Adaptive Mesh Refinement (AMR) technique with a refinement strategy based on local volume density and Jeans length. The smallest cell size spans 0.05 pc in the most refined regions, which is thus the minimum softening scale for both the gas and the stars formed during the simulation.

The equations of motions and hydrodynamics are solved by the RAMSES code (Teyssier 2002). The gas follows a piecewise polytropic equation of state (EoS) fitting the heating/cooling equilibrium (see Kraljic et al. 2014, and references therein). A Jeans polytrope sets a pressure floor in the most refined volumes, to prevent artificial fragmentation. We refer the reader specifically to Sections 2.2, 2.3 and 4.2 of R+13 and Kraljic et al. (2014) for further discussions on this and specific EoS (see Robertson & Kravtsov

2008; Tasker & Bryan 2008; Dobbs et al. 2011; Bonnell et al. 2013, for a few other implementation schemes). The resulting gas density probability distribution function (PDF) (McKee & Ostriker 2007, and references therein) in the present simulation follows a classic log-normal shape (Nordlund & Padoan 1999; Padoan & Nordlund 2002) with an additional few percents of the mass in a power-law tail at high density (R+13, Choi et al. (2013)), as expected from gravity and observed in real molecular clouds and galaxies (Lombardi et al. 2010; Druard et al. 2014). While changes in the AMR grid refinement can locally bias the velocity dispersion, the density and velocity power spectra are thus clearly dominated by a single turbulence cascade with a well-identified injection scale at the average Jeans length (Bournaud et al. 2010, R+13). The very high resolution of the present simulation allows to resolve the turbulent cascade with a realistic power spectrum (R+13, Combes et al. (2013)) and density distribution (Druard et al. 2014) down to the parsec scale.

The simulation comprises conversion of gas into stellar particles (down to $160 M_\odot$) where the volume density ρ_0 exceed 2000 cm^{-3} , assuming that the local star formation rate depends on the free-fall time and with the star formation efficiency set at 3% (R+13). This recipe does not take into account additional physics that may impact on the formation of molecules, and we thus rely on the equation of state to follow the cloud collapse, the low temperatures and the high density which triggers the formation of new stars. These newly formed “stars” are evolved on the AMR grid, i.e. with gravitational softening down to 0.05 pc, much smaller than the dark matter and primordial stellar components. The implementation of stellar feedback includes photoionisation through heating, radiative pressure via injection of momentum, and supernova explosions in the kinetic form (see R+13 for more details). A more thorough study of the impact of resolution or metallicity in such simulations was conducted by Kraljic et al. (2014), who have shown that the artificial density threshold ρ_0 does not tune the efficiency of star formation, which mostly depends on the turbulence level (e.g., Mach number, see Klessen 2000; Li et al. 2004; Audit & Hennebelle 2010; Renaud et al. 2012).

The artificial viscosity induced by the refinement process is also not expected to induce e.g., spurious fuelling even close to the potential resonances in such a simulation. Introducing a new refinement level induces some additional dispersion within the new cells which are created. That dispersion is itself not a true turbulence term. The power spectrum is in fact dominated by the injection of turbulence from the large scale, and the higher resolution in these new cells also allow the gas to cool further. The thermal energy is thus replaced by kinetic energy but this does not induce turbulence per se. A simple calculation pertaining to the present simulation can provide some further estimate of this process. Assuming a mean free path of one cell, with velocities associated with sound waves, we can estimate an upper limit of the (viscous) acceleration in an homogeneous medium as $a_{\text{visc}} = (c_s dv/dr)/2$ (with c_s the sound speed). At the resonance (~ 500 pc), the gas is dense, with densities around 100 H/cc , hence dv/dr is of the order of $50 \text{ km.s}^{-1}.\text{kpc}^{-1}$ which leads to $a_{\text{visc}} \sim 0.03 \text{ pc.Myr}^{-2}$ (for $c_s \sim 1 \text{ km s}^{-1}$). This estimate would significantly decrease if we were to consider the realistic filling factor of real gas clouds (and not an homogeneous medium). The energy (E) dissipation rate for the turbulence per unit mass at the resonance is then $dE/dt = 3/2 \sigma^2/\tau$ where $\sigma \sim 10 \text{ km s}^{-1}$ is the one-dimensional turbulence (root mean square) and τ the free-fall time ($\sim 5 \text{ Myr}$ for densities around 100 H/cc). We then get the acceleration associated with the turbulence via $a_{\text{turb}} = 3 \sigma^2 / (2\tau \cdot V)$. With $V \sim 100 \text{ km s}^{-1}$ at

the resonance, this leads to $a_{\text{turb}} \sim 0.3 \text{ pc.Myr}^{-2}$. Hence, artificial viscosity would have a negligible role in the triggering of gas fuelling, even close to the resonances.

The results presented in this paper focus on the fueling due to the stellar bar which forms during the simulation, and the associated evolution of the inner region, down to the vicinity of the black hole. We have conducted two runs at two different resolutions following the same initial conditions. The first simulation (or run) is as described in R+13 and reaches its maximum resolution of 0.05 pc (refinement level 21) in a number of very dense regions. Within the bar, that maximum resolution is only reached late in the simulation just before its end time at about $t = 800 \text{ Myr}$. This motivated the launch of a second run at slightly coarser resolution (cells of about 1 pc, with a maximum level of refinement of 17) to pursue the evolution of the central region for an additional 30 Myr (i.e., about the dynamical time-scale at a radius of 1 kpc or 10 dynamical time-scales at 100 pc).

In the following, all measurements and maps derived from snapshots prior to $t = 800 \text{ Myr}$ are therefore using the original simulation (R+13), with the others extracted from the simulation at 1 pc resolution (for the gaseous component). Note that star formation was turned on at $t \sim 745 \text{ Myr}$ in the simulation as to avoid gas being prematurely consumed. Details on the implemented recipes for star formation, stellar feedback (photoionisation, radiative pressure, supernova explosions) are described in R+13. Adding on AGN feedback would significantly impact on the distribution, kinematics and physical status of the gas, specifically for the close environment of the black hole (Ciotti & Ostriker 1997; Haehnelt et al. 1998; Silk & Rees 1998; Kauffmann & Haehnelt 2000). For the present simulations, however, we do not include the potential feedback from an active galactic nucleus (AGN), thus focusing on a time window ($t \sim 750 - 830 \text{ Myr}$) when we consider that the AGN itself is quiet (or in an “off-state”). This is partly justified by the assumption that AGN have low duty cycle at low redshift and for black holes of a few $10^6 M_\odot$ (Haehnelt & Rees 1993; Wang et al. 2009; Shankar et al. 2010, 2013) and by the short time range we are considering. More importantly, it allows us to narrow down our study to probe the interplay between the dynamical evolution and the effect of star formation (similarly to e.g., Levine et al. 2008; Hopkins & Quataert 2010a). Turning on the AGN in such a simulation would be paramount to understand any potential fueling cycle starting from the large-scale down to the vicinity of the black hole, and such an implementation has already been included in RAMSES by a direct calculation of the Bondi accretion rate (see Teyssier et al. 2011; Gabor & Bounaud 2014, and references therein). It would nevertheless require to probe various feedback schemes, and triggering mechanisms, which is beyond the scope of the present paper.

3 RESULTS

In the following, we roughly reconstruct the chronology of events as witnessed in the simulation. The large-scale bar forms, fuels gas towards the centre and the inner Lindblad resonance, creating a spiral-like structure and a ring, with part of this gas spiraling down to the inner few parsecs around the black hole, triggering star (cluster) formation. The new stellar cluster and the black hole are bound to each other, and wander away from the center of gravity of the older stellar population. This symmetry breaking event speeds up the fragmentation of the ring, triggering further localised starbursts in clumps as well as in the close vicinity of the black hole. Part of the gas is expelled tens of parsecs away from the galactic plane

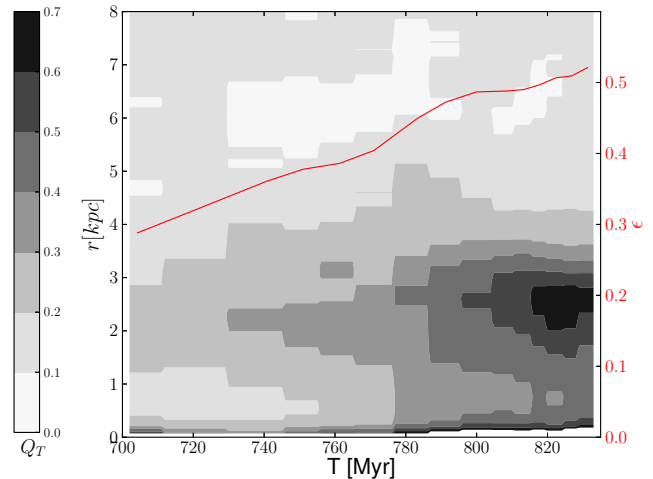


Figure 1. Tangential to radial force ratio $Q_T(r)$ (left y axis) for different snapshots of the simulation presented with respect to time (in Myr), and radius (left label in kpc). The amplitude of Q_T is colour-coded and the correspondence is provided in the colourbar at the left of the plot. The time variation of the ellipticity of the bar is provided as a red solid line (labels on the right).

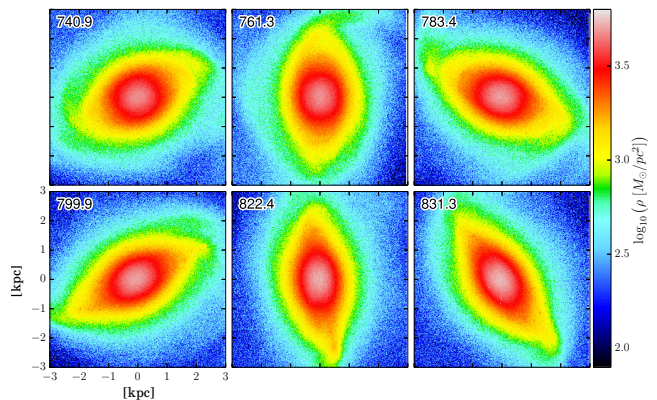


Figure 2. Face-on view of the surface (mass) stellar density within 3 kpc of the simulation for 6 snapshots showing the evolution of the large-scale stellar bar. The snapshot time (in Myr) is indicated in the upper left corner of each panel.

via stellar feedback, and is accreted back within an inclined disc of about 10 pc around the black hole. That out-of-the-plane accretion induces further star formation in the close vicinity of the central dark mass. These events are detailed in the following Sections.

3.1 Bar formation and gas fueling

3.1.1 The bar formation

The bar is already formed at $t = 700 \text{ Myr}$, and dominates the old stellar component within the central 3 kpc (R+13). It stills grows significantly until the end of the simulation run at 830 Myr: this is shown in Figure 1 by the time variation of the force ratio $Q_T(r) = |F_T(r, \theta)|_{\text{max}} / \langle |F_r(r, \theta)| \rangle$ (Combes & Sanders 1981; Buta & Block 2001). The maximum amplitude $Q_b = \max[Q_T(r)]$ goes from about 0.2 (weak bar, see e.g., Eskridge et al. 2002; Buta & Block 2001; Buta et al. 2004, 2006) at 700 Myr to ~ 0.65 (strong bar) at 830 Myr, while the bar (two-dimensional) ellipticity

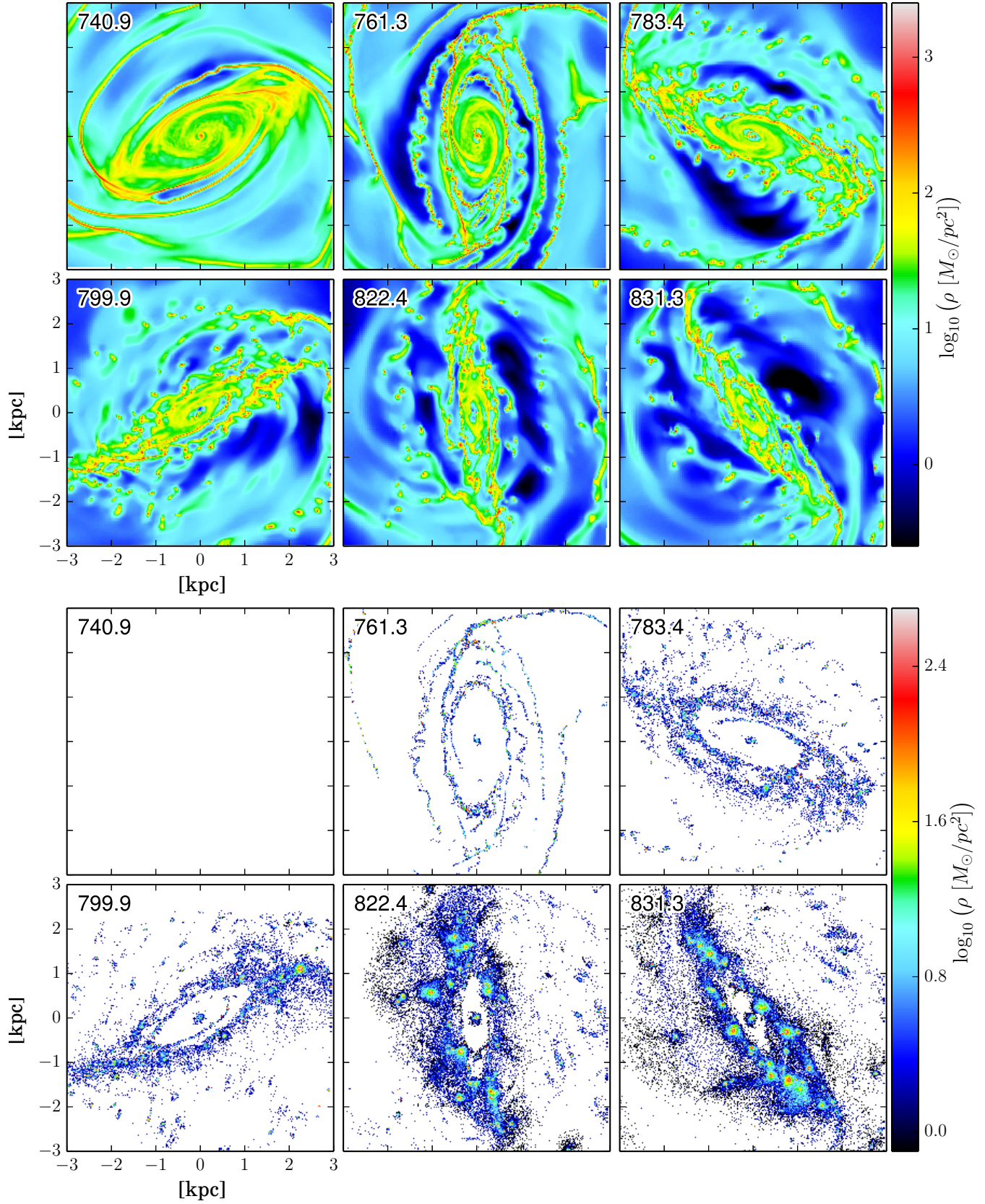


Figure 3. Same as in Fig. 2 but for the gas (upper 6 panels) and all stars formed during the simulation (lower 6 panels). The top left panel ($t = 740.9$ Myr) stays blank as the star formation was not yet turned on at that stage of the simulation (see Sect. 2).

increases from 0.3 to 0.5. The maximum amplitude is reached at a radius of about 2.6 kpc. As mentioned in R+13, the bar pattern speed Ω_b is about $58 \text{ km s}^{-1} \text{ kpc}^{-1}$, while the outer spirals are slower with $\Omega_{\text{spiral}} \sim 50 \text{ km s}^{-1} \text{ kpc}^{-1}$. The bar corotation lies at $\sim 3.6 \text{ kpc}$ at 800 Myr. The bar exerts strong torques which act on the gas by driving radial outflows and inflows. As emphasised in R+13, inner resonances appear while the bars forms, with radii of ~ 40 and 450 pc . In the rest of this paper, we focus on the evolution and central gas radial redistribution due to the bar, namely within the central $\sim 3 \text{ kpc}$.

3.1.2 The bar evolution

With a pattern speed of $\sim 58 \text{ km s}^{-1} \text{ kpc}^{-1}$, the bar rotates by about 45° every $\sim 13 \text{ Myr}$, as illustrated in Fig. 2: the ellipticity increase of the bar (Fig. 1) thus occurs here in less than a rotation period. The gas is significantly redistributed via the bar formation along spiral shocks connecting at the end of the bar (Fig. 3), which then follow several embedded banana-shaped thin structures: this seems to follow the expected orbits around the Lagrangian points, as described by e.g., Athanassoula (1992) and Maciejewski et al. (2002). Three or four of these thin overdensities meet near both ends of the stellar bar where the outer spirals start. They also curve towards the centre resulting in a irregular ring-like structure at a radius of about 400 pc. The standard bi-symmetry expected in idealised simulations (see e.g., Maciejewski et al. 2002) is broken here with superimposed $m = 1$ and $m = 3$ modes: these are visible both in the stellar component (Fig. 2) as well as in the three-arms gaseous overdensity at a radius of $\sim 500 \text{ pc}$ in Fig. 3. At the end of the bar, gas densities go up to $\sim 10^4 \text{ M}_\odot \cdot \text{pc}^{-2}$, while it is on average less than $10^3 \text{ M}_\odot \cdot \text{pc}^{-2}$ in the inner spirals. More diffuse gas with densities of $[20 - 50] \text{ M}_\odot \cdot \text{pc}^{-2}$ is present within the bar, filling the inter-arm regions. As the bar evolves and its ellipticity increases, the inner gaseous structure gets also more elongated, but keeps a relatively regular appearance with only the spiral and shock lanes outside the bar getting disrupted. Part of this disruption may be due to the density gradient and Rayleigh-Taylor instabilities (see e.g. Maciejewski et al. 2002) but also to the local shear and Kelvin-Helmholtz instabilities.

3.1.3 The lack of star formation within the bar

Within 3 kpc, stars form at an average rate of about $0.1 \text{ M}_\odot \cdot \text{yr}^{-1}$. As expected, the star formation sites generally trace the overdensities described above. There is, however, a remarkable exception: apart from a very centralised burst inside 40 pc (see Sect. 3.2.1), the region inside the bar (the inner kiloparsec or so) is devoid of new stars except in the central $\sim 100 \text{ pc}$. As illustrated in the bottom panel of Fig. 3, star formation proceeds efficiently at the very edge of the bar, with the presence of many clumps following x_1 orbits along the bar. There are also two additional clump concentrations at the two ends of the bar. Within the bar itself, stars solely form either along a couple of thin curvy streams or at the very centre.

Considering the significant morphological changes of the bar (Fig. 2) and within the bar (Fig. 3), it is difficult to directly assess the mass budget evolution in that region. A reasonable estimate can still be obtained by following the variation of position angle and ellipticity of the density from the old stellar population, and using that to measure the enclosed mass. The cumulated mass of gas and new stars within an elliptical region with a major-axis of 500 pc (the average ellipticity of that region being 0.25) is almost constant with $1.8 \cdot 10^7 \text{ M}_\odot$, all new stars ($\sim 4 \cdot 10^6 \text{ M}_\odot$) being formed

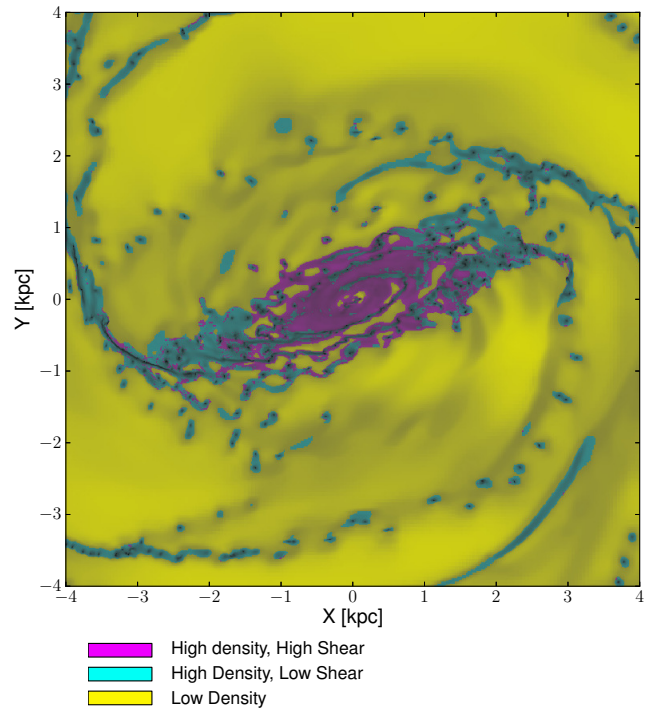


Figure 4. Map of the 8 central kpc of the simulation showing both information about surface density and shear at $t = 800 \text{ Myr}$. Low density gas is coded in yellow. High density gas with high (resp. low) shear is coded in magenta (resp. cyan). The map clearly shows that high shear, high density gas is strictly confined to the inner region of the bar.

within the central 40 pc (see Sect. 3.2.1). The fact that star formation is not triggered within the inner region of the bar despite gas densities being above $10^3 \text{ M}_\odot \cdot \text{pc}^{-2}$ is quite remarkable. This could originate either in processes preventing gas to collapse and form stars within the bar region despite the high densities, or by the absence of processes needed to trigger star formation. Potential scenarios may involve cloud-cloud collisions as emphasised by Fujimoto et al. (2014), which should be particularly important at the bar ends and in the outer spiral. To explain the low star formation rate within the bar, intrinsic difference in the cloud properties (e.g., concentration) are invoked, but it does not directly point out the required physical origin for such differences (but see Kruijsen et al. 2014).

Stars thus form in the bar convergence region and principal shocks where there is a slight associated increase of gas density (Fig. 3). However, the difference between dense regions of gas within the bar which form stars or not is only marginally associated with the gas density itself: at a scale of 10 pc, the regions devoid of star formation within the bar are of similar or even higher densities than the star forming ones at the end of the bar or in the spiral. The present simulation distinctly shows such a well confined low star formation rate within a bar. We should therefore have a closer look at the bar-driven gas flows to seek whether or not the mentioned behaviour can be associated with the very specific (and complex) orbital and dynamical structure induced by the bar. In a dynamical context, one of the local ingredients which could prevent gas clouds to collapse is shear, namely forces which would tear down coherent gas structures, acting as a dynamically disruptive agent on gas clouds.

We probed this hypothesis by calculating the normalised shear

at a scale of about 5 pc (refinement level 14). Namely, we compute the quadratic sum of the non-diagonal terms of $F_{\alpha,\beta} = dV_{\alpha}/d\beta - dV_{\beta}/d\alpha$ where α and β represent two of the three cartesian coordinates (x, y, z), and then calculate the mass-weighted average of that quantity normalised by the local gas self-gravity. In Fig. 4, we present a map of the local normalised shear: regions with low density are represented in yellow, and regions with high density are in cyan or magenta, the former being associated with low shear while the latter emphasises high shear regions (the gas density is also coded in the map brightness, higher density regions being darker). High density gas, namely with a volume density larger than about 2000 cm^{-3} , corresponds to the power-law tail of the probability density function (see R13), hence should thus be self-gravitating and is expected to collapse and form stars if no other mechanism opposes it.

Small star forming clumps around or outside the bar are all in regions of low shear. There is in fact an excellent correspondence between the location of high density clumps at low shear and the regions where the new stars form (see Fig. 3): the spiral arms are thus all clearly flagged in cyan in Fig. 4, as well as the two ends of the bar. The inner region of the bar, besides a small area around the very centre, is strikingly singled out in Fig. 4 as having both high gas densities and high shear. This is a strong hint that shear may be a significant actor in preventing star formation to occur within the bar, except at the very centre which we probe further in the next Sections.

3.2 The central kpc

We now focus on the environment of the black hole within the inner resonances where the gas is funnelled: the inner 100 pc is a region of active star formation (as opposed to its immediate surroundings within the bar).

3.2.1 Evolution of the inner ring

The central structures associated with the bar inner Lindblad resonances are formed early with a clear spiral-like morphology established by $t = 730$ Myr (Figs. 3 and 5). The fueling rate is steady within 100 pc at a level of $0.02 \text{ M}_{\odot} \cdot \text{yr}^{-1}$ or less (Fig. 7). The two incoming arms connect to the central 40 pc disc-like structure, respectively reaching surface densities of about 400 and $250 \text{ M}_{\odot} \cdot \text{pc}^{-2}$. As the gas accumulates, the arms then continue down to a few parsecs distance from the black hole. Such structures may be reminiscent of the gas distribution obtained in some hydrodynamical simulations in the presence of a bar where the presence of an additional central mass can drive the propagation of a spiral down to the very centre, albeit with significantly lower amplitudes (see e.g. Englmaier & Shlosman 2000) or via an idealised scheme (Maciejewski 2004a,b). These studies include a fixed (tumbling) potential while the present simulations includes live stellar and dark matter components, star formation and feedback.

The gas distribution evolves rapidly with sometimes three armlets linking the small and large-scale structure (Fig. 5). The inner Lindblad resonance ring at 40 pc is most visible at $t \sim 750$ Myr, and has an average radial thickness of about 10 pc. Most of the new stars within 100 pc form in that thick ring. At $t \sim 755$ Myr, the wrapping of the inner spiral forms a secondary elongated ring-like gas distribution with a radius of about 85 pc. This is quite visible in e.g., the top right panel of Fig. 6 where the in-plane velocity vectors are superimposed on the gas density maps. Within the in-

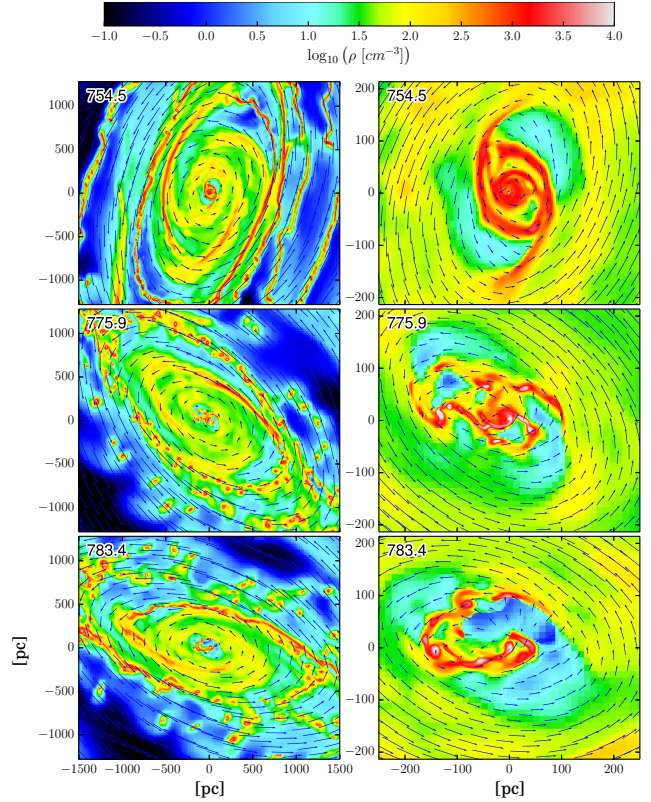


Figure 6. Three snapshots of the gas volume density maps at 1 kpc (left panels) and 200 pc (right panels) scales, with the gas velocity flow superimposed as blue arrows.

ner Lindblad resonance ring (40 pc), the gas inflow is almost exactly cancelled by the star formation rate of about $10^{-3} \text{ M}_{\odot} \cdot \text{yr}^{-1}$, meaning that the gas mass enclosed within that radius stays relatively constant until $t = 770$ Myr (Fig. 7). Between 50 and 100 pc, the gas inflow rate is high enough to pursue the building of the central gas mass concentration despite new stars being continuously formed. Between $t = 765$ and 770 Myr, the gaseous mass within 100 pc reaches its peak with about $3.1 \cdot 10^6 \text{ M}_{\odot}$, a value similar to the black hole mass itself.

In the present simulation, the ring starts to fragment when about $3 \cdot 10^6 \text{ M}_{\odot}$ of gas has been gathered within the central structure (see Fig. 7). As most of this gas is confined within a vertical layer of 10 to 20 pc, it represents nearly 50% of the background stellar mass within the same radial extent and height (and is similar to the mass of the black hole). The break of the regular inflowing gaseous pattern triggers the formation of about ten clumps most of them embedded in filamentary over-densities. The mass of gas and stars within each clump ranges between 0.5 and $1.5 \cdot 10^5 \text{ M}_{\odot}$ (derived within a radius of 10 pc around the density peak of each clump) and an average mass of 10^5 M_{\odot} . This is a very rapidly evolving phase, with the clumps individually interacting with each other and with the background potential (including the black hole). This leads to the disruption of most of these clumps on a timescale shorter than 15 Myr, with 10^6 M_{\odot} of gas being further fueled within the central 20 pc and almost entirely converted into new stars. By $t \sim 780$ Myr, the inner regular disc and ring have disappeared leaving a very concentrated peak of gas and new stars surrounding the black hole within a radius of about 5 pc. Such an instability is naturally expected considering that the central gas disc

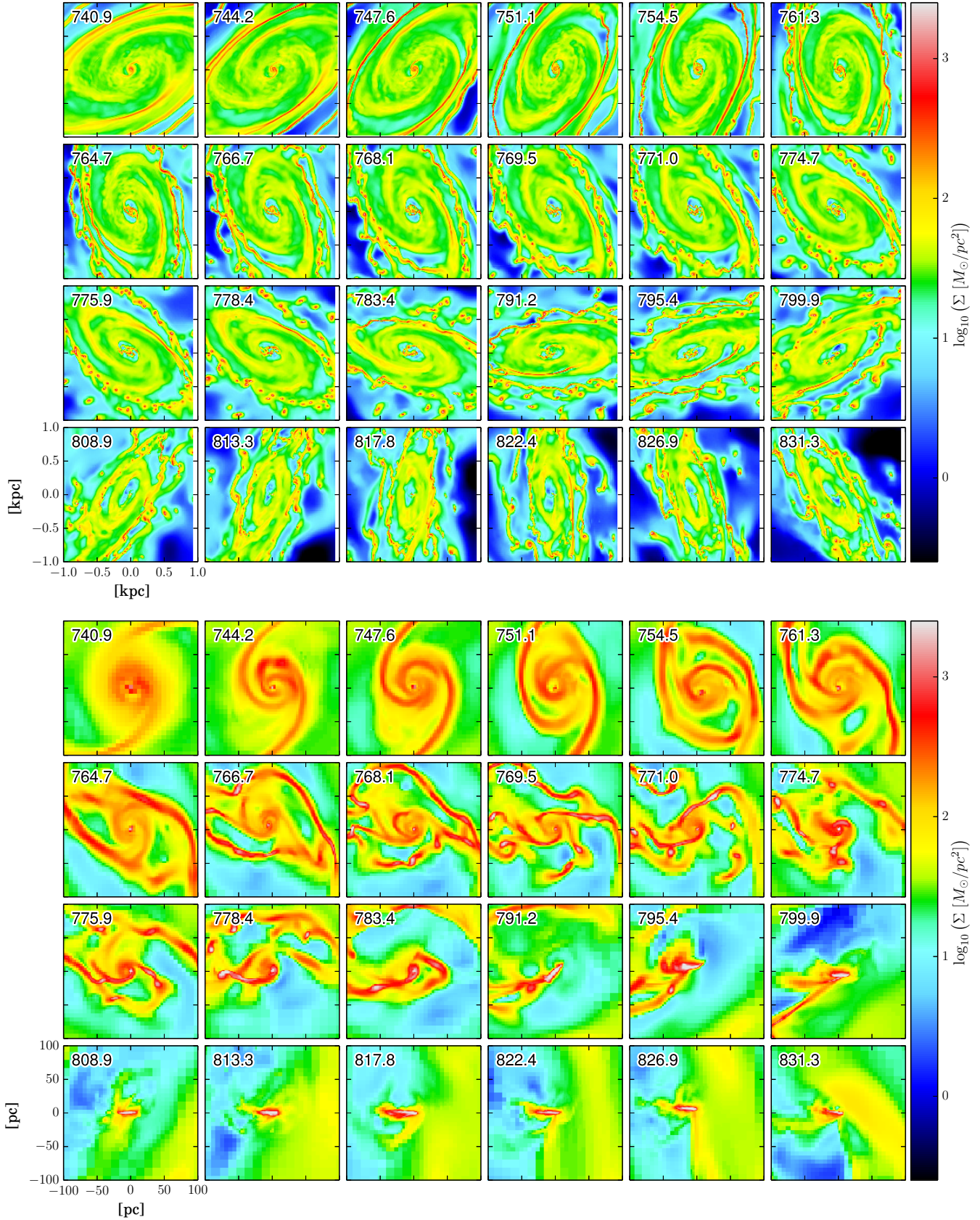


Figure 5. Face-on view of the gas surface density distribution within the central 1 kpc (top panels) and 100 pc (bottom panels). Each set of 24 panels show about 90 Myr of evolution with an average of about 4 Myr between each panel. The time (in Myr) of each snapshot is indicated at the top left corner of each panel. The black hole is centred in all panels. The 20 pc size structure seen in the bottom panels after ~ 800 Myr is a vertical disc structure (see Sect. 3.2.3).

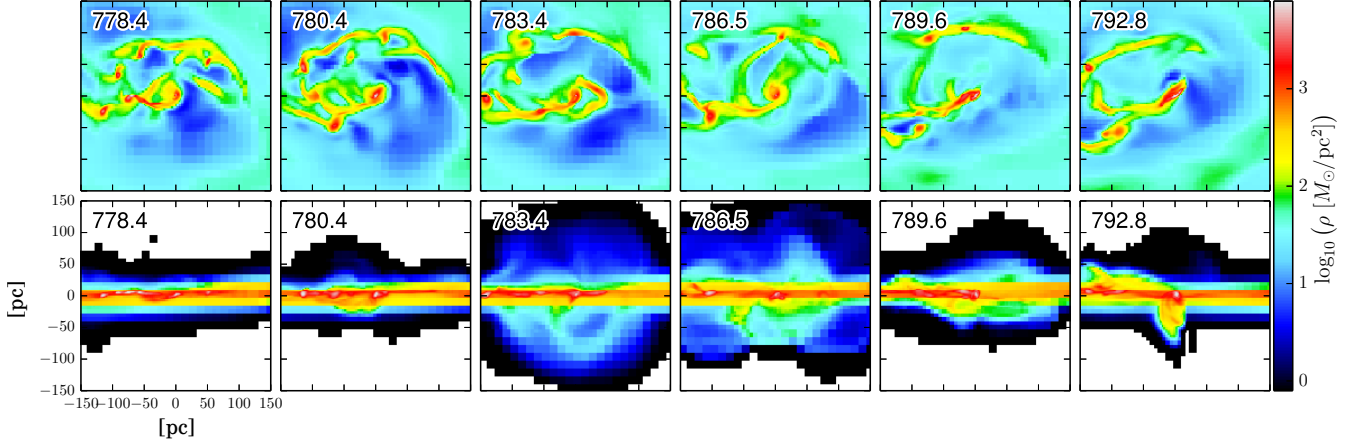


Figure 8. Six snapshots over about 15 Myr with face-on (first row) and edge-on (second row) views of the gas in the central 150 pc. The impact of stellar feedback, which creates bubble-like cavities and filaments away from the main plane, is clearly visible.

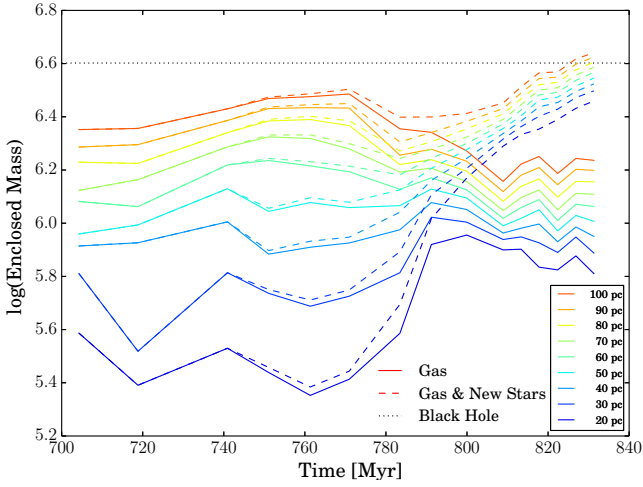


Figure 7. Enclosed mass (M_\odot in \log_{10}) within a spherical region centred around the black hole with respect to time in the simulation: the colour coding corresponds to various radii. The solid lines represent the gas alone, the dashed lines are for the gas plus stars formed during the simulation, and the dotted black line indicates the mass of the supermassive black hole, as a reference.

and the new stars weigh more than the central dark mass itself and become self-gravitating. However, one of the triggering ingredients of this violent phase is associated with the motion of the black hole, which is emphasised in the next Section. Such a violent and rapid evolution may naturally lead to a rapidly time-varying fueling of the black hole itself, hence explain the intermittency in the Active Galactic Nuclei (AGN) activity (Hopkins & Quataert 2010a; Gabor & Bounaud 2013).

3.2.2 The coupling of the black hole and the nuclear cluster

As mentioned in Sect. 3.1.2 and in Fig. 3, the stellar bar is not perfectly symmetric and shows some lopsidedness (significant $m = 1$ mode, see Jog & Combes 2009, and references therein). The centre of mass of the central kiloparsec does in fact moves around as the bar rotates, with a maximum amplitude of the order of 50 pc. The central black hole initially follows the centre of gravity of the inner region of the bar rather accurately until $t \sim 760$ Myr.

As gas piles up in the central 100 pc, star formation starts within a very compact region around the black hole, and a stellar cluster slowly forms (at a few $10^{-3} M_\odot \cdot \text{yr}^{-1}$) initially with a radius R_N of less than 10 pc. As a first approximation, we can evaluate the timescale for the black hole to exchange energy with the cluster by deriving the dynamical friction time (see e.g. Merritt 2013): $T_{df} \sim 5 \cdot 10^9 \cdot (\sigma_f/100 \text{ km} \cdot \text{s}^{-1})^3 \cdot (\rho/10^5 M_\odot \text{pc}^{-3})^{-1} \cdot (m/10 M_\odot)^{-1} \cdot (\ln \Lambda/10)^{-1} \text{ yr}$. For a cluster of $10^5 M_\odot$ within a radius of 10 pc, a measured dispersion of 40 km s^{-1} , and a black hole of $4 \cdot 10^6 M_\odot$, T_{df} is shorter than 1 Myr. The relaxation time t_R of the cluster itself is significantly longer (~ 15 Myr) as it approximately scales as $t_R \sim \sqrt{R_N^3/GM} \times (N/8 \log(N))$, where N is the number of particles representing new stars. The accreted gas mass and the compact stellar cluster newly formed around the black hole tend to couple these components on a rather short timescale. This further tends to decouple the motion of the central gaseous disc, cluster of new stars and black hole from the centre of gravity of the older stellar population of the bar which precesses with time.

The decoupling has a direct and significant effect on the gaseous ring as the larger-scale fueling and resonance structure slowly shifts away from the central black hole, and breaks the symmetry of the orbital structure and gaseous flow. It can easily be seen in Fig. 5: around $t = 767$ Myr, the ring fragments while the whole gaseous distribution becomes strongly asymmetric. The increasing offset of the black hole further amplifies the violent evolution of the gas structure described in the previous Section. It is thus interesting to note that after $T \sim 765$ Myr the formation of clumps within the central 100 pc is in fact initially the consequence of the black hole and cluster offsetting, and not solely from the local gas over-density and self-gravity.

3.2.3 Star formation in clumps, and stellar feedback

Star formation is triggered in the densest regions, which include a few of these clumps, but also the filamentary overdensities which represent the left-overs of the inner Lindblad ring. The star formation in these clumps sums up to about $2 \cdot 10^{-3} M_\odot \cdot \text{yr}^{-1}$ within 100 pc. The clumps are organised within a twisted elliptical structure with a diameter of about 250 pc, and a vertical extension of 20 pc, the black hole being offset by about 70 pc from its centre (Figs 5 and 8). As mentioned, the following fast evolution tends to both disrupt these structures, and make them merge within the cen-

tral 20 pc. By $t \sim 780$ Myr, only a few clumps remain as all have been disrupted or merged with the very central overdensity. This triggers a rapid density increase after $t = 790$ Myr and a subsequent ten fold increase of the star formation rate: it is clearly visible in Fig. 7 as the mass of gas enclosed in 20 and 100 pc respectively first decreases and then increases rapidly: in the later step the mass within 20 pc goes from $\sim 8\%$ to $\sim 45\%$ of the mass within 100 pc (excluding the black hole). The inflow is associated with a net increase of the star formation rate which reaches $0.05 \text{ M}_{\odot} \cdot \text{yr}^{-1}$, almost entirely focused in the very close environment of the black hole. This is to be compared with the star formation rate at the end of the bar of a few $\text{M}_{\odot} \cdot \text{yr}^{-1}$. The violent evolution of the gas distribution also constrains the availability of gas directly fueling the black hole: this could be a natural cause of AGN variability in galaxies on timescales of a few Myr.

Another important ingredient for the evolution of the central structure is the feedback associated with the starburst in the clumps. Following the prescriptions implemented in the simulation, this feedback concerns 20% of the formed stellar mass. It first takes the form of a photo-ionisation bubble and radiative pressure, followed by supernova explosions (via injection of kinetic energy) activated 10 Myr after new stars are formed. The stellar feedback expels gas outside the main plane and up to about 200 pc as illustrated in Fig. 8. It creates a large expanding bubble (see third snapshot in Fig. 8), the gas ultimately falling back onto the disc in a few Myrs, part of it being caught in the environment of the black hole. A rather thin nearly vertical gaseous disc with an extent of about 20 pc is thus being formed (Fig. 9), which continues to slowly accrete gas and form stars. Gas clouds being accreted close to the black hole are tidally stretched during their course¹, creating a series of extended tidal-like features (from 5 to 50 pc in size) precessing within the vertical disc: this can be seen in Fig. 9 but is best illustrated when only the dense gas is shown as in Fig. 13. These filaments may be associated with the streamers observed at the centre of the Milky Way (see discussion in Sect. 4.3). The stellar-driven feedback thus helps remove angular momentum from the gas, and allows it to come closer to the supermassive black hole. In this regard, it is important to notice that it is the asymmetry of gas infall after star formation feedback, which produces the lopsidedness of the gas distribution in the center of the galaxy: this was already alluded to by Rodríguez-Fernández & Combes (2008), who argued that the asymmetry of the central potential is insufficient to account for the observed lopsidedness.

3.2.4 The nuclear star cluster

The above-mentioned evolution involves several subsequent episodes of star formation around the black hole. During the first phase ($t \lesssim 760$ Myr), stars forming within 100 pc of the black hole are the result of the radial inward motion of the gas associated with the resonance ring, building a nuclear star cluster of a few 10^5 M_{\odot} . Most of these stars have thus an overall angular momentum vector aligned with the one of the main galaxy disc. Only stars within the inner 5 pc have a more isotropic motion, following the nearly spherical potential imposed by the black hole. In a second phase, after $t \sim 790$ Myr, new stars form from gas which has been expelled via stellar-driven feedback and been re-accreted in a gaseous disc-like structure, perpendicular to the galaxy plane.

¹ See the extreme case of a highly stretched gas cloud around the Milky Way black hole in Gillessen et al. (2013).

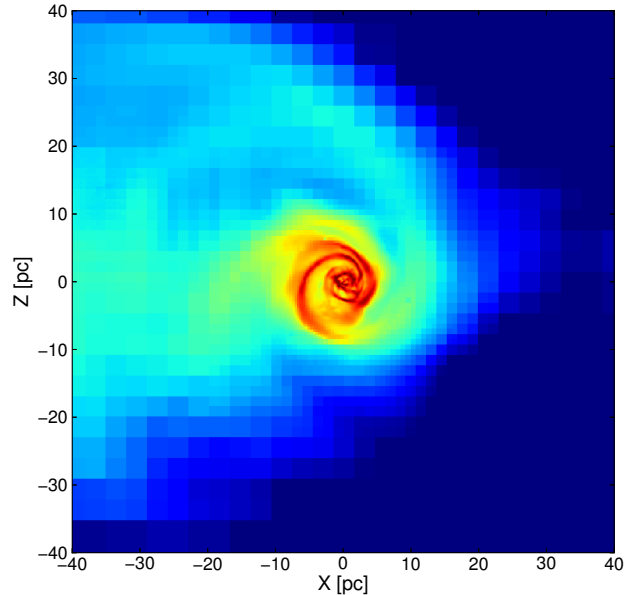


Figure 9. Nearly face-on view (X, Z) of the accretion within the 40 pc around the black hole at $t = 830$ Myr: note that this view corresponds to an edge-on view of the main galaxy plane (X, Y).

These new stars have a well-organised rotation with velocities going from 30 to 130 km s^{-1} between 3 and 10 pc (see Fig. 10), and velocity dispersions between 8 and 15 km s^{-1} . Within the central 2 pc, we observe more counter-rotating stars and the dispersion becomes larger than the mean azimuthal velocity. The gas distribution and velocities at a scale of 10 pc exhibit an off-centring (see Figs. 9 and 10) which can be associated with an $m = 1$ mode, naturally expected for a potential dominated by a point mass (e.g. Masset & Tagger 1997; Hopkins & Quataert 2010a). The averaged angular momentum vector of this inclined disc lies within the large-scale galactic plane. The newly formed stars are thus superposed with the slightly older, hotter and more isotropic population of stars formed in the first phase as illustrated in Fig. 11. At the end of the simulation ($t \sim 830$ Myr), the nuclear star cluster is therefore made up of several generations of stars, the youngest having an average angular momentum vector oriented within the galaxy plane (perpendicular to the total angular momentum vector of the galaxy), while the older have a more spherical and isotropic distribution (Figs. 11 and 12). This is reminiscent of the recent observations by Feldmeier et al. (2014) who witnessed the potential presence of a set of stars orbiting perpendicularly with respect to the Galactic plane. More generally, it may lead to a natural explanation for multiple stellar populations with different kinematic signatures in the central regions of galaxies, even though the time window within which such signatures can be observed should be addressed.

4 DISCUSSION AND CONCLUSIONS

4.1 Chronology and structures

We now summarise the chronology of events observed within the simulations and mentioned in the last Sections, to emphasise a few important ingredients and processes. It is important to emphasise again here that most detected features within the bar are rapidly evolving and thus transient.

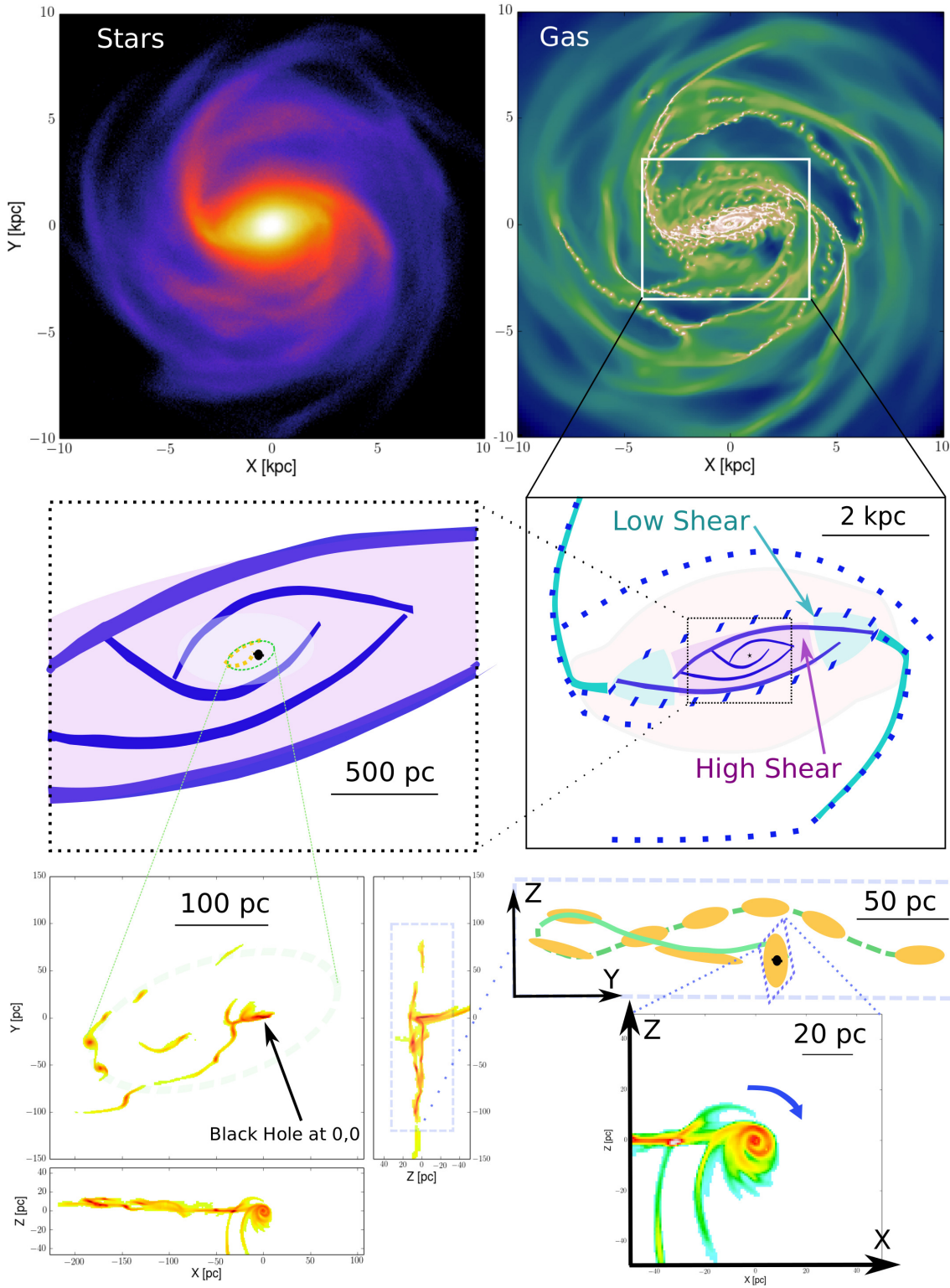


Figure 13. Combined set of sketches and maps emphasising the structures observed in the simulation at various scales. Top panels: the stellar (left) and gaseous (right) mass distributions within 10 kpc, seen face-on. Middle panels: sketches illustrating the structures, including star forming clumps (blue dots), gas spirals and lanes (green and purple curved lines). The background colors delineate the bar (pale red), and regions with low and high shear within the bar (as in Figure 4). Bottom left panels: face-on (X, Y), edge-on (X, Z) and end-on (Y, Z) views of the gas within the central ~ 200 pc emphasising the dense gas clouds and their asymmetric distribution at $t \sim 800$ Myr. Note also the vertical extent of the ring-like structure seen in the edge-on and end-on view. Bottom right panels: illustration of the torus-like ring and its clumps of dense gas connected to the vertical disc surrounding the black hole.

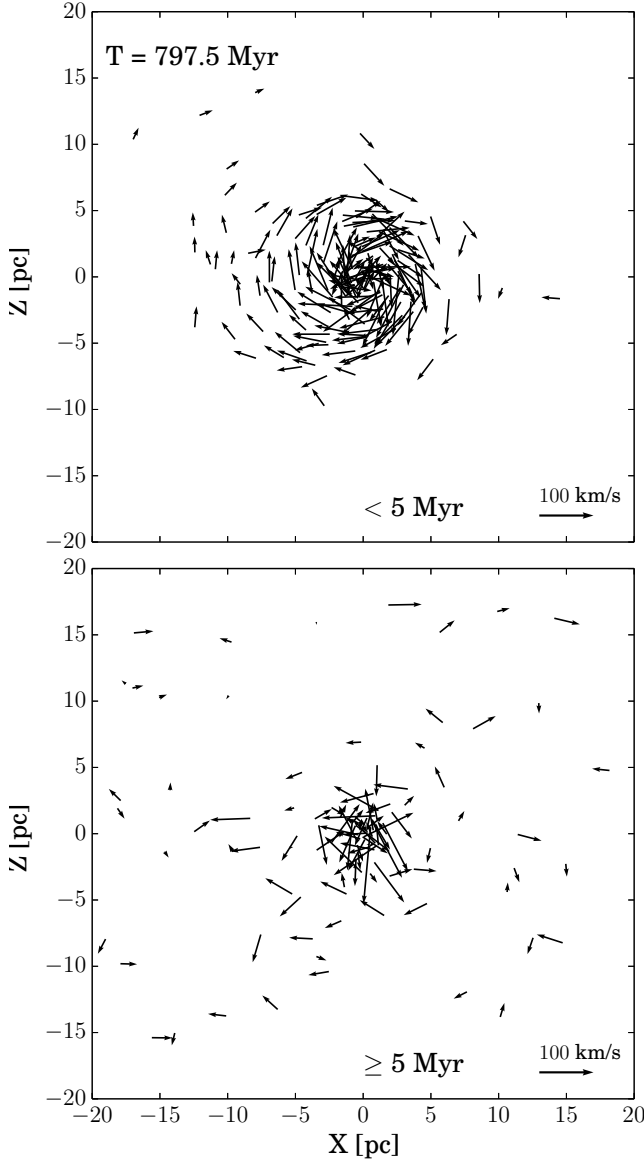


Figure 10. Inner X, Z view of the (formed) stars positions and velocities in the central 20 pc around the black hole at $t \sim 800$ Myr. Arrows correspond to the velocities in the X, Z plane (the velocity scale is indicated at the bottom right). The top (resp. bottom) panel corresponds to more recently, < 5 Myr, (resp. earlier, > 5 Myr) formed particles.

- Despite the presence of a significant amount of gas within the bar region, star formation proceeds mostly at its ends, or within a radius of about 100 pc near the black hole and not in between;
- Resonant structures (Lindblad) focus gas in elongated ring-like distributions, themselves connected to the central dark mass via mini-spirals within a few tens of parsecs;
- Gas clumps of a few $10^5 M_\odot$ are rapidly forming as a consequence of the gas accumulation and symmetry breaking described in Sect. 3.2.2. However, only the most massive clumps manage to efficiently form stars, and they rapidly get disrupted;
- Star formation and stellar feedback are important ingredients which allow the gas to be transported at higher heights, part of it falling back to be accreted into a dense structure around the black hole. AGN feedback could in principle play a comparable role.
- The resulting inner elliptical (ring-like) structure with a diam-

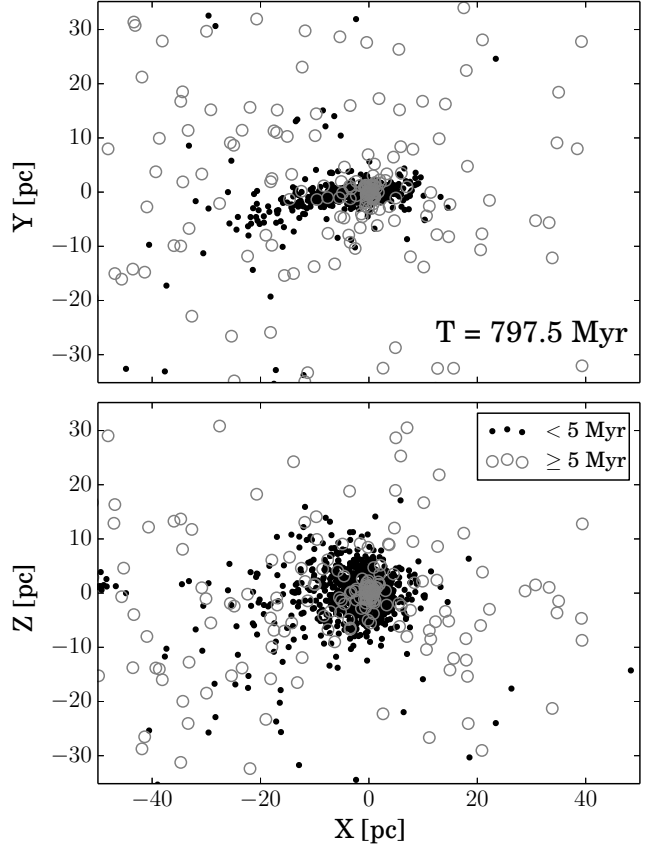


Figure 11. X, Z and X, Y views of the stars formed during the simulation within 40 pc at $t \sim 800$ Myr, splitted in two age bins (< 5 Myr, black dots; > 5 Myr, open grey circles). The very young stars are mostly distributed within a disc-like structure which is perpendicular to the main galaxy plane (X, Y). Note the core of stars older than 5 Myr, and its more extended and flattened distribution.

eter of about 250 pc exhibits a vertical extension of 10 to 20 pc, the black hole being offset by about 70 pc from its centre.

- Gas accreted around the black hole within a radius of about 10 pc is distributed in a disc-like structure decoupled from the main Galactic plane, with its angular momentum vector aligned within the main galactic plane.
- The gas accreted in the vicinity of the black hole is stretched by the associated tidal forces, creating a series of long winding tails of gaseous material.

To better illustrate the corresponding scales and structures, we use $t \sim 795$ Myr as a reference time and present the actual stellar and gas distributions with sketches flagging the most important features in Fig. 13. At a scale of a few kiloparsecs, the bar and associated spiral arms dominate. Star formation mostly proceeds in the spiral arms (see Renaud et al. 2013; Kraljic et al. 2014, for details) and at the ends of the bar, as discussed in Sect. 3.1.3. A series of intertwined gas filaments connect the ends of the bar down to the central 250 pc where the gas partly ends in a thick pseudo-ring surrounding a lower density region. The gas structures continue inwards with thinner spiral arms connecting with the central 50 pc ring and disc seen in Fig. 5. In the simulation we present here, about $2 \cdot 10^7 M_\odot$ of gas is accumulated within a radius of 200 pc around the black hole, a few $10^6 M_\odot$ within 100 pc (see Fig. 7), and about $2 \cdot 10^5 M_\odot$ within the 10 pc radius vertical disc. As emphasised in

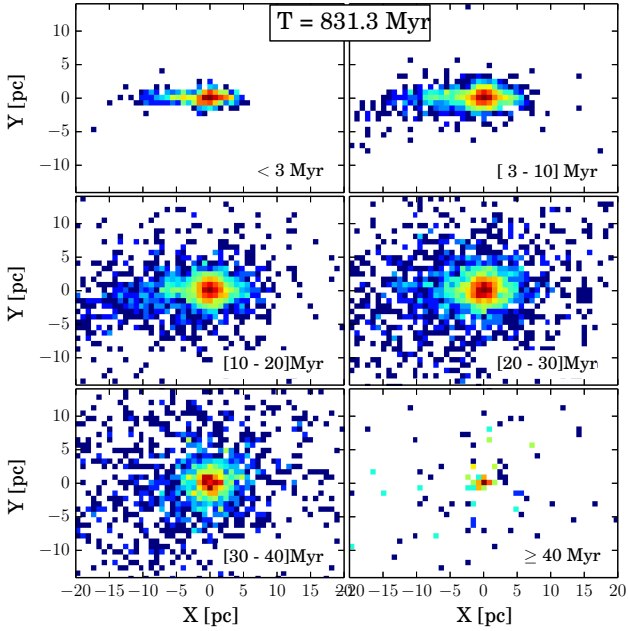


Figure 12. X, Y views of the stars formed during the simulation within 20 pc at $t \sim 830$ Myr separated by ages. Panels go from younger than 3 Myr (top left) to older than 40 Myr (bottom right).

Fig. 7, the gas mass within the 100 pc stays relatively constant as star formation proceeds. The accelerated fueling rate in the central 200 pc occurs when the instability sets in, thus breaking the ILR barrier (see also, Englmaier & Shlosman 2004). Hence it is the combination of the bar-driven fueling, the lack of star formation in the bar, and the onset of the instability at the centre, which manages to bring gas in the close vicinity of the black hole: these three processes are thus followed simultaneously within the present simulation which then leads to the formation of a polar disc at a scale of 10 pc around the black hole.

4.2 Limitations of the simulation

It is important to probe whether the results and processes described above are specific to the considered simulation, with its characteristics (e.g., spatial and mass resolutions, numerical scheme) and implemented recipes (star formation, stellar-driven feedback). We thus briefly review processes which may be significantly affected by varying prescriptions.

Even though the morphology and evolution of resonance rings certainly depend on the details pertaining to the mass profile, gas content, etc, the large-scale fueling of gas towards resonances is a generic property of bars (Athanassoula 1992; Combes 2001). In the present simulation, the existence of a central spiral fueling the inner region is associated with the presence of a central dark mass as theoretically expected (see e.g. Fukuda et al. 1998) and observed (Combes et al. 2013, 2014; Garcia-Burillo et al. 2014). The exact evolutionary steps followed by the gas distribution at the very centre (Fig. 5) are nevertheless closely linked to the star formation and feedback implemented schemes. It may also heavily depend on the prior presence of a massive stellar cluster around the black hole, as such a seed cluster would imply a more diffuse mass distribution and a consequently less peaked velocity gradient, at least in the central few tens of parsecs.

The relative impact of shear on the local gas densities inside

the bar (Sect. 3.1.3, Fig. 4), at its ends and outside may vary, both in terms of the properties of the bar itself and the physical ingredients included in the simulation and its detailed implementation. In the inner regions, it seems, however, hard to prevent high shear for medium to high strength bars considering that it is a direct consequence of the orbital structure in the bar combined with the dissipative nature of the gas. Measurements of shear for clouds within actual bars would help confirm this picture.

Another set of limitations originates in the treatment of the non-dissipative particles, namely the old stars, dark matter and the massive black hole. These are evolved on a sub-grid with an associated spatial softening of 3 pc, hence coarser than the grid following the very dense gas regions. New stars form with a mass of a few hundreds solar masses, thus not sampling a given initial mass function but always representing an indissociable group of simultaneously born stars. Additionally, the cartesian (adaptive) grid itself may impose some alignment in the observed structures which may partly impact on the vertical orientation of the central disc structure around the black hole (Hahn et al. 2010; Dubois et al. 2014). However, the vertical structure is mostly set by the angular momentum of the incoming gas: the nuclear disc is in fact not initially aligned with the grid main axes, and its symmetry axis shifts with time, going away from the grid orientation. At the end of the simulation, most of the mass in that disc is concentrated within a radius of 10 pc, about 200 times the smallest resolution element and gas is being accreted from larger scale filaments which are not aligned with the inner disc. Last but not least, supernovae feedback is provided at a constant rate which depends directly on the mass of new stars, and is not described as a stochastic event. These ingredients certainly impact on the interaction between e.g., the dense gas clumps and the new stellar populations. It thus affects the relaxation at the very centre between the new stars and the black hole. This may consequently induce a different evolutionary path for the central region: the importance of each event in the chronology described above should therefore be probed via different simulations starting with various prescriptions and initial conditions.

4.3 Other barred galaxies and our Milky Way

We finally wish to relate the various features and evolution witnessed in the simulation with structures actually observed in our own Milky Way or in external galaxies. We first start by briefly pointing out the lack of star formation in the inner part of the bar (Sect. 3.1.3).

The classification of barred galaxies following the spatial distribution of their HII regions generally leads to two or three groups (Phillips 1996; Verley et al. 2007). Various authors thus emphasised the lack of star formation within the bar region for early-type galaxies (SBb and SBa) with strong bars. An early study of NGC 1530 beautifully shows such a concentration of star forming regions solely at the ends of the galactic bar or around the nucleus (Reynaud & Downes 1998): the authors argued for the role of bar-induced shear as the source for the disruption of potential star forming clouds. The lack of star formation within the bar region despite the presence of diffuse gas therefore seems to be a rather common property of disc galaxies with strong bars. Phillips (1996) and Martin & Friedli (1997) also point out that these systems often exhibit a starbursting nuclear region very probably associated to inner resonances, a prototypical example being NGC 1300 (see also Elmegreen et al. 2009, and references therein).

In our own Galaxy, studies of actual Galactic giant molecular clouds like W43 (Carlhoff et al. 2013; Motte et al. 2014) seem to

indicate low shear values for dense clouds lying close to the end of the Galactic bar, where heightened star formation occurs. On the other hand, Longmore et al. (2013) pointed out the very low level of star formation down to a radius of about 500 pc. The inner 500 pc region, labelled Central Molecular Zone (CMZ), seems to harbour high densities of gas, but with very little star forming sites. Longmore et al. (2013) and Kruijssen et al. (2014) have thus argued that the star formation rate within the CMZ is significantly below what is expected considering the amount of high-surface density gas.

Going further inward, the inner dense molecular structure is often described as an elliptical and twisted ring of semi major-axis 100 pc (Molinari et al. 2011). SgrA seems to be offset from this ring by about 50 pc. The distribution of dense gas is not symmetric along that ring as emphasised by recent maps of cold dust and gas clouds (e.g. Molinari et al. 2011; Liu et al. 2013). The presence of gas streamers was also recently reexamined by (Liu et al. 2012), who nicely illustrated (see their Fig. 7) the connection between a central molecular ring a few parsecs in size and larger-scale gas filaments which seems to be tidally distorted and coiled.

All these features are qualitatively reminiscent of the ones observed at the 200 pc and 10 pc scales in the present simulation (see Figs. 9 and 13): the twist of the ring formed by the few clumps at a scale of about 150 pc, distributed asymmetrically around the black hole, which itself is surrounded by accreted infalling gas, some of it being stretched by tidal forces. The fact that some of the scales are similar (the size of 100 pc ring, the offset of the black hole) is certainly a coincidence. However, the fact that such structures naturally emerge from relatively generic processes (gas accretion, dynamical friction and dissipation, star-driven feedback) hints for new avenues to probe the formation and evolution processes of galactic nuclei. We should also emphasise the case of M83 (Thatte et al. 2000; Díaz et al. 2006; Houghton & Thatte 2008) which hosts a bar resembling the one in the present simulation, and has an intriguing asymmetric circumnuclear region. The latter has been interpreted as the signature of a transient $m = 1$ mode (Knapen et al. 2010), the result of a complex startburst episode (Piqueras López et al. 2012), or of an accretion event (Rodrigues et al. 2009): the observed central structures in M83 could thus be reconsidered in the light of the simulation we presented in this paper.

At the end of the simulation described in the present paper, the bar is still slowly growing. It is therefore impossible to robustly address its long term evolution. Nevertheless, one of the most important characteristics of the features observed in the simulation described above is their transient nature: redistribution of gas and its fuelling towards the central region, building up of the mass in the vicinity of the black hole, star formation and stellar-driven feedback all occur within a time window shorter than 100 Myr. The central structures significantly evolve on an even shorter timescale, namely a few Myr, under the strong influence of instabilities and the motion of the black hole. This could be a natural source of intermittency for the fueling of the black hole itself, hence partly causing the time-varying nature of AGN Hopkins & Quataert (2010a); Gabor & Bournaud (2013). We could also speculate that after the violent phase which resulted in the formation of a nuclear (vertical) disc around the black hole, the gas flow driven by the bar tumbling potential would resume. This could be the starting point for a second cycle with in-spiraling gas being accumulated in a ring or disc-like structure at a scale of 100-200 pc, hence triggering another episode of rapid evolution where the black hole, and stellar-driven feedback would play a major role. Such a two-phase scenario is clearly reminiscent of the one proposed in a pioneer-

ing paper by Shlosman et al. (1989), where gas is first transported from kpc down to pc scales via dynamical instabilities, accumulating mass within an inner gaseous disc which could then become unstable and provide fuel to an existing black hole (or form one). Qualitatively similar cycles have also been proposed by e.g., Kruijssen & Longmore (2013) as a potential mechanism to explain the rather low efficiency of star formation in the CMZ. We emphasise here the critical roles of the central dark mass and of the symmetry breaking for the evolution of the structures, as well as the importance of feedback for the redistribution of angular momentum.

The present study thus illustrates the importance of the interplay between large-scale and small scale dynamics, and the potential richness initiated by the presence of a bar, a black hole, gas dynamics, star formation and the associated feedback. If a second cycle were to be triggered, a number of key ingredients would naturally differ in the initial conditions. The potential of the bar itself is changing with time, and is being influenced by the exchange of angular momentum between the stars and the gas (Bournaud et al. 2005). The central mass distribution and dynamics should also be significantly different, and the central black hole may be expected to grow in mass (something we did not follow in the present simulation). Still, the formation of resonant structures at scales of about 100 pc and smaller, followed by gravitational instabilities, the formation of gas clumps, star formation, outflow and re-accretion closer to the black hole could be generic features for gas-rich spiral galaxies. If such cycles occur, as already nicely emphasised by e.g., Stark et al. (2004), our simulation suggests that they would span time periods of $\sim 100 - 200$ Myr. Their detailed properties and evolutionary tracks will obviously depend on many ingredients including the relative mass of the black hole and the availability of gas. This would certainly condition the mode of accretion onto the black hole, but also its time variability.

Similar time-varying structures have been witnessed in simulations by Hopkins & Quataert (2010a) Levine et al. (2008), or Mayer et al. (2010). Hopkins & Quataert (2010a) used “zooming-in” techniques to reach sub-parsec scales in a series of simulations varying the gas fraction and treatments of the gas feedback. Some of their simulations develop one-arm spirals with a clumpy structure (namely Nf8h1c0 in Hopkins & Quataert 2010b), but these are for very gas-rich systems (mass fraction of gas within 100 pc of about 0.5) with high accretion rates of a few $M_{\odot} \text{ yr}^{-1}$ inside 100 pc, so that the clumpiness directly derives from the gas self-gravity. Overall, the simulations presented and discussed in Hopkins & Quataert (2010b,a) show a rather smooth gaseous distribution within the central 100 pc, but as emphasised by Hopkins & Quataert (2010b), this heavily depends on the implemented stellar-driven feedback recipe, as well as on the imposed cooling floor. Levine et al. (2008) also used a zoom-in technique to reach cell sizes as small as 0.03 pc in a simulated disc galaxy within a cosmological volume. A range of instabilities and spiral structures are observed from kpc to pc scales. A circumnuclear self-gravitating gas disc forms during the simulation and has a remarkably constant power-law density profile. Both Hopkins & Quataert (2010a) and Levine et al. (2008) depict a situation where large-scale gas inflows are orders of magnitude higher than in the simulation we describe in the present paper. As for the study of Mayer et al. (2010), a merger-driven gas inflow is followed with a spatial resolution down to a tenth of a parsec: the onset of an unstable massive disc around the supermassive black hole is even more rapid, hence a very high corresponding accretion rate.

The main specific attribute of the simulation we present here is then the relatively quiet accretion mode at the 100 pc scale

($\leq 0.02 \text{ M}_{\odot} \text{ yr}^{-1}$), even though we witness a rapidly evolving structure within the central 200 pc. We self-consistently follow this evolution (while ignoring any potential AGN feedback process) with the formation of a decoupled 10 pc scale (polar) circumnuclear structure which may be of high relevance for the evolution of galactic nuclear regions. In that context, high resolution hydrodynamical simulations specifically focusing on few parsecs domains have also been used to study the interaction between infalling gas clouds and a black hole (see e.g. Lucas et al. 2013; Alig et al. 2013) in an attempt to better understand the complex stellar and gaseous morphologies and dynamics observed near the Galactic centre. More recent constraints on their formation processes come from the observations of e.g., Feldmeier et al. (2014) who managed to map the detailed stellar kinematics of the central cluster, and suggest the existence of a stellar perpendicular structure within the inner 1 pc. Considering the connections and coupling between the various scales and processes, as emphasised in the present paper, it would thus be important to examine such issues with self-consistent simulations at very high mass and spatial resolutions.

ACKNOWLEDGEMENTS

We would like to warmly thank Yohan Dubois and Romain Teyssier for useful input which helped the writing of this paper. We thank Diederick Kruijssen for his input on the final stages of the manuscript. F. Renaud, F. Bournaud and J. Gabor acknowledge support from the EC through grant ERC-StG-257720. This work was granted access to the PRACE Research Infrastructure resource Curie hosted at CEA-TGCC, France (PRACE project ra-0283-, and national GENCI resources, projects 2013-GEN2192 and 2014-GEN2192).

REFERENCES

- Alig C., Schartmann M., Burkert A., Dolag K., 2013, *ApJ*, 771, 119
- Athanassoula E., 1992, *MNRAS*, 259, 345
- Audit E., Hennebelle P., 2010, *A&A*, 511, 76
- Binney J., Gerhard O. E., Stark A. A., Bally J., Uchida K. I., 1991, *MNRAS*, 252, 210
- Bonnell I. A., Dobbs C. L., Smith R. J., 2013, *MNRAS*, 430, 1790
- Bournaud F., Combes F., Semelin B., 2005, *MNRAS*, 364, L18
- Bournaud F., Elmegreen B. G., Teyssier R., Block D. L., Puerari I., 2010, *MNRAS*, 409, 1088
- Buta R., Block D. L., 2001, *ApJ*, 550, 243
- Buta R., Laurikainen E., Salo H., 2004, *AJ*, 127, 279
- Buta R., Laurikainen E., Salo H., Block D. L., Knapen J. H., 2006, *AJ*, 132, 1859
- Carlhoff P., et al., 2013, *A&A*, 560, 24
- Choi J.-H., Shlosman I., Begelman M. C., 2013, *ApJ*, 774, 149
- Choi E., Naab T., Ostriker J. P., Johansson P. H., Moster B. P., 2014, *MNRAS*, 442, 440
- Ciotti L., Ostriker J. P., 1997, *ApJL*, 487, L105
- Cisternas M., et al., 2013, *ApJ*, 776, 50
- Combes F., 2001, in *Advanced Lectures on the Starburst-AGN Connection*. p. 223, <http://adsabs.harvard.edu/abs/2001sac.conf..223C>
- Combes F., Sanders R. H., 1981, *A&A*, 96, 164
- Combes F., et al., 2013, *A&A*, 558, 124
- Combes F., et al., 2014, *A&A*, 565, 97
- Díaz R. J., Dottori H., Aguero M. P., Mediavilla E., Rodrigues I., Mast D., 2006, *The Astrophysical Journal*, 652, 1122
- Dobbs C. L., Burkert A., Pringle J. E., 2011, *MNRAS*, 417, 1318
- Druard C., et al., 2014, *A&A*, 567, 118
- Dubois Y., et al., 2014, *arXiv:1402.1165*
- Elmegreen B. G., 1993, *ApJL*, 419, L29
- Elmegreen B. G., Galliano E., Alloin D., 2009, *ApJ*, 703, 1297
- Englmaier P., Shlosman I., 2000, *ApJ*, 528, 677
- Englmaier P., Shlosman I., 2004, *ApJL*, 617, L115
- Eskridge P. B., et al., 2002, *ApJS*, 143, 73
- Feldmeier A., et al., 2014, *arXiv:1406.2849*
- Fujimoto Y., Tasker E. J., Wakayama M., Habe A., 2014, *MNRAS*, 439, 936
- Fukuda H., Wada K., Habe A., 1998, *MNRAS*, 295, 463
- Gabor J. M., Bournaud F., 2013, *MNRAS*, 434, 606
- Gabor J. M., Bournaud F., 2014, *MNRAS*, 441, 1615
- Garcia-Burillo S., et al., 2014, *arXiv:1405.7706*
- Gillessen S., et al., 2013, *ApJ*, 774, 44
- Haan S., Schinnerer E., Emsellem E., García-Burillo S., Combes F., Mundell C. G., Rix H.-W., 2009, *ApJ*, 692, 1623
- Haas M. R., Schaye J., Booth C. M., Dalla Vecchia C., Springel V., Theuns T., Wiersma R. P. C., 2013, *MNRAS*, 435, 2931
- Haehnelt M. G., Rees M. J., 1993, *MNRAS*, 263, 168
- Haehnelt M. G., Natarajan P., Rees M. J., 1998, *MNRAS*, 300, 817
- Hahn O., Teyssier R., Carollo C. M., 2010, *MNRAS*, 405, 274
- Hopkins P. F., Quataert E., 2010a, *MNRAS*, 405, L41
- Hopkins P. F., Quataert E., 2010b, *MNRAS*, 407, 1529
- Houghton R. C. W., Thatte N., 2008, *MNRAS*, 385, 1110
- Jog C. J., Combes F., 2009, *Phys. Rep.*, 471, 75
- Jogee S., 2006, in . eprint: *arXiv:astro-ph/0408383*, p. 143, doi:10.1007/3-540-34621-X'6, <http://adsabs.harvard.edu/abs/2006LNP...693..143J>
- Jogee S., Scoville N., Kenney J. D. P., 2005, *ApJ*, 630, 837
- Kauffmann G., Haehnelt M., 2000, *MNRAS*, 311, 576
- Klessen R. S., 2000, *ApJ*, 535, 869
- Knapen J. H., Sharp R. G., Ryder S. D., Falcón-Barroso J., Fathi K., Gutiérrez L., 2010, *MNRAS*, 408, 797
- Kraljic K., Renaud F., Bournaud F., Combes F., Elmegreen B., Emsellem E., Teyssier R., 2014, *ApJ*, 784, 112
- Kruijssen J. M. D., Longmore S. N., 2013, *MNRAS*, 435, 2598
- Kruijssen J. M. D., Longmore S. N., Elmegreen B. G., Murray N., Bally J., Testi L., Kennicutt R. C., 2014, *MNRAS*, 440, 3370
- Levine R., Gnedin N. Y., Hamilton A. J. S., Kravtsov A. V., 2008, *ApJ*, 678, 154
- Li P. S., Norman M. L., Mac Low M.-M., Heitsch F., 2004, *ApJ*, 605, 800
- Liu H. B., Hsieh P.-Y., Ho P. T. P., Su Y.-N., Wright M., Sun A.-L., Minh Y. C., 2012, *ApJ*, 756, 195
- Liu H. B., Ho P. T. P., Wright M. C. H., Su Y.-N., Hsieh P.-Y., Sun A.-L., Kim S. S., Minh Y. C., 2013, *ApJ*, 770, 44
- Lombardi M., Alves J., Lada C. J., 2010, *A&A*, 519, L7
- Longmore S. N., et al., 2013, *MNRAS*, 429, 987
- Lucas W. E., Bonnell I. A., Davies M. B., Rice W. K. M., 2013, *MNRAS*, 433, 353
- Maciejewski W., 2004a, *MNRAS*, 354, 883
- Maciejewski W., 2004b, *MNRAS*, 354, 892
- Maciejewski W., Teuben P. J., Sparke L. S., Stone J. M., 2002, *MNRAS*, 329, 502
- Martin P., Friedli D., 1997, *A&A*, 326, 449
- Masset F., Tagger M., 1997, *A&A*, 322, 442

- Mayer L., Kazantzidis S., Escala A., Callegari S., 2010, *Nature*, 466, 1082
- McKee C. F., Ostriker E. C., 2007, *ARAA*, 45, 565
- Merritt D., 2010, *ApJ*, 718, 739
- Merritt D., 2013, *Dynamics and Evolution of Galactic Nuclei*, Princeton Series in Astrophysics edn. David N. Spergel, Series Editor, <http://adsabs.harvard.edu/abs/2013degn.book.....M>
- Molinari S., Bally J., Noriega-Crespo A., Compiègne M., et al. 2011, *ApJL*, 735, L33
- Motte F., et al., 2014, *ArXiv e-prints*, 1404, 4404
- Nordlund Å. K., Padoan P., 1999, in *Interstellar Turbulence*. p. 218, <http://adsabs.harvard.edu/abs/1999intu.conf..218N>
- Padoan P., Nordlund Å., 2002, *ApJ*, 576, 870
- Padoan P., Nordlund Å., 2011, *ApJ*, 730, 40
- Phillips A. C., 1996, in *Barred galaxies*. Astronomical Society of the Pacific Conference Series, Proceedings of a conference held at the University of Alabama; Tuscaloosa; Alabama, p. 44, <http://adsabs.harvard.edu/abs/1996ASPC...91...44P>
- Piqueras López J., Davies R., Colina L., Orban de Xivry G., 2012, *ApJ*, 752, 47
- Renaud F., Kraljic K., Bournaud F., 2012, *ApJL*, 760, L16
- Renaud F., et al., 2013, *MNRAS*, 436, 1836
- Reynaud D., Downes D., 1998, *A&A*, 337, 671
- Roberts W. W. J., Huntley J. M., van Albada G. D., 1979, *ApJ*, 233, 67
- Robertson B. E., Kravtsov A. V., 2008, *ApJ*, 680, 1083
- Rodrigues I., Dottori H., Díaz R. J., Agüero M. P., Mast D., 2009, *AJ*, 137, 4083
- Rodríguez-Fernandez N. J., Combes F., 2008, *A&A*, 489, 115
- Shankar F., Crocce M., Miralda-Escudé J., Fosalba P., Weinberg D. H., 2010, *ApJ*, 718, 231
- Shankar F., Weinberg D. H., Miralda-Escudé J., 2013, *MNRAS*, 428, 421
- Shlosman I., Frank J., Begelman M. C., 1989, *Nature*, 338, 45
- Silk J., Rees M. J., 1998, *A&A*, 331, L1
- Stark A. A., Martin C. L., Walsh W. M., Xiao K., Lane A. P., Walker C. K., 2004, *ApJL*, 614, L41
- Tasker E. J., Bryan G. L., 2008, *ApJ*, 673, 810
- Teyssier R., 2002, *A&A*, 385, 337
- Teyssier R., Moore B., Martizzi D., Dubois Y., Mayer L., 2011, *MNRAS*, 414, 195
- Thatte N., Tecza M., Genzel R., 2000, *A&A*, 364, L47
- Verley S., Combes F., Verdes-Montenegro L., Bergond G., Leon S., 2007, *A&A*, 474, 43
- Wada K., Habe A., 1995, *MNRAS*, 277, 433
- Wang J.-M., et al., 2009, *ApJL*, 697, L141